Supplementary Material

For reader's convenience and for the sake of completeness, we add this supplementary material to present the values of the various SDCs. In Appendix A, we present the numerical values for the various SDCs in the improved NRQCD factorization. In Appendix B, we derive the SDCs of the traditional NRQCD factorization from the improved one, and present the their numerical values.

Before the whole appendix, we first present the classification of diagrams in detail. Fragmentation diagrams represent a sum of diagrams where gluon exchanges inside each J/ψ produced by a single photon, as illustrated in FIG.1. All the other diagrams are classified into non-fragmentation diagrams.

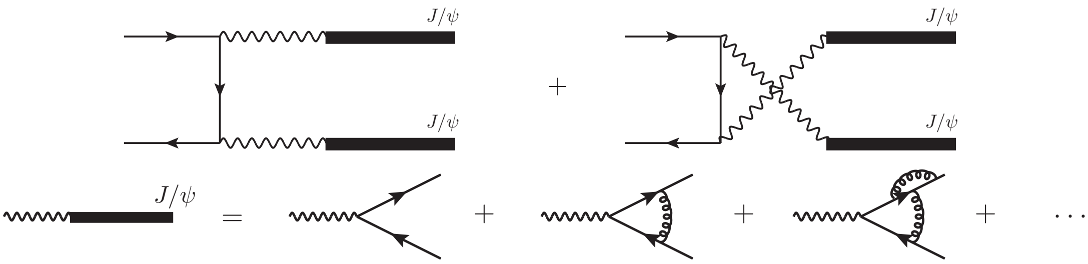

FIG. 1: Illustration of the $e^+e^- \to J/\psi J/\psi$ process through two photon independent fragmentation.

Appendix A: Numerical results for various SDCs in improved NRQCD factorization

For reader's convenience, we have tabulated in Table A.1 all the SDCs through $\mathcal{O}(\alpha_s^2)$ that enter Eq. (7), for ten different values of $\cos\theta$. For completeness, we have also listed the values of $\mathcal{C}_{\rm fr}$, the analytical expression of which are given in Eq. (6). In the last column in Table A.1, we split $\hat{c}_{\rm nfr}^{(2)}$ into two terms which have different sources, the inner product between the two-loop non-fragmentation amplitude and the tree-level non-fragmentation amplitude, and the absolute square of the one-loop non-fragmentation amplitude, respectively. We clearly see that only $\mathcal{C}_{\rm fr}$ exhibits strong angular dependence. The non-fragmentation SDCs $\mathcal{C}_{\rm nfr}$ are always insignificant for entire range of θ. The importance of the interference term $\mathcal{C}_{\rm int}$ increases as $\cos\theta$ decreases. Since the SDCs $\hat{c}_{\rm int}^{(1,2)}$ have negative sign, including higher-order radiative corrections turn to dilute the destructive interference effect.

$\cos\theta$	$\mathcal{C}_{\rm fr}$ (GeV^{-4})	$\mathcal{C}_{\rm int}^{(0)}$ (GeV^{-4})	$\hat{c}_{\rm int}^{(1)}$	$\hat{c}_{\rm int}^{(2)}$	$\mathcal{C}_{\rm nfr}^{(0)}$ (GeV^{-4})	$\hat{c}_{\rm nfr}^{(1)}$	$\hat{c}_{\rm nfr}^{(2)}$
0.999	4.163	−0.334	−3.62	−71.75	0.006	−7.42	$-143.174 + 42.974 = -100.20$
0.970	3.646	−0.242	−1.34	−76.57	0.007	−6.33	$-146.117 + 37.424 = -108.69$
0.872	1.573	−0.193	−0.73	−80.64	0.008	−5.07	$-152.144 + 25.321 = -126.82$
0.775	0.988	−0.176	−1.27	−81.77	0.010	−5.11	$-155.633 + 19.124 = -136.51$
0.677	0.722	−0.164	−1.85	−82.00	0.011	−5.49	$-157.716 + 15.969 = -141.75$
0.531	0.522	−0.152	−2.58	−81.67	0.012	−6.15	$-159.349 + 14.092 = -145.26$
0.384	0.422	−0.143	−3.12	−81.08	0.012	−6.73	$-160.032 + 13.777 = -146.26$
0.287	0.383	−0.139	−3.38	−80.71	0.012	−7.03	$-160.222 + 13.898 = -146.32$
0.140	0.350	−0.135	−3.63	−80.31	0.012	−7.32	$-160.324 + 14.160 = -146.16$
0	0.340	−0.133	−3.70	−80.17	0.012	−7.41	$-160.341 + 14.271 = -146.07$

TABLE A.1: Numerical values of various SDCs in Eq. (7) through $\mathcal{O}(\alpha_s^2)$ for ten different values of $\cos\theta$.

Appendix B: Perturbative corrections to $e^+e^- \to J/\psi J/\psi$ in traditional NRQCD factorization

In this appendix, we also show the results for the perturbative corrections $e^+e^- \to J/\psi J/\psi$ from the standard NRQCD factorization approach. We take the shortcut to arrive at Eq. (3) directly from the improved NRQCD factorization predictions. Setting $M_{J/\psi} = 2m_c$ in Eq. (5), and expressing the decay constant $f_{J/\psi}$ in terms of $\langle \mathcal{O} \rangle_{J/\psi}$ in accordance with Eq. (8), we can rewrite the differential cross section as

$$\frac{d\sigma}{d\cos\theta} = \frac{1}{2s}\frac{\beta}{16\pi}\frac{e^8 e_c^4}{4}\mathcal{F}^{(0)}\left[1 + \frac{\alpha_s}{\pi}f^{(1)} + \left(\frac{\alpha_s}{\pi}\right)^2\left(f^{(1)}\frac{\beta_0}{4}\ln\frac{\mu_R^2}{m_c^2} + 4\gamma_{J/\psi}\ln\frac{\mu_\Lambda^2}{m_c^2} + f^{(2)}\right)\right]\frac{\langle \mathcal{O}\rangle_{J/\psi}^2}{m_c^2}, \tag{B.1}$$

where

$$\mathcal{F}^{(0)} = \mathcal{C}_{\rm fr} + \mathcal{C}_{\rm int}^{(0)} + \mathcal{C}_{\rm nfr}^{(0)}, \tag{B.2a}$$

$$f^{(1)} = \tilde{f}^{(1)} + \frac{2\mathfrak{f}^{(1)}}{\mathcal{F}^{(0)}}\mathcal{C}_{\rm int}^{(0)} + \frac{\mathcal{C}_{\rm int}^{(0)}\hat{c}_{\rm int}^{(1)} + \mathcal{C}_{\rm nfr}^{(0)}\hat{c}_{\rm nfr}^{(1)}}{\mathcal{F}^{(0)}}, \tag{B.2b}$$

$$f^{(2)} = \tilde{f}^{(2)} + \frac{(\mathfrak{f}^{(1)})^2}{\mathcal{F}^{(0)}}\mathcal{C}_{\rm int}^{(0)} + \frac{2\mathfrak{f}^{(2)}}{\mathcal{F}^{(0)}}\mathcal{C}_{\rm int}^{(0)} + \frac{2\mathfrak{f}^{(1)}}{\mathcal{F}^{(0)}}\mathcal{C}_{\rm int}^{(0)}\hat{c}_{\rm int}^{(1)} + \frac{\mathcal{C}_{\rm int}^{(0)}\hat{c}_{\rm int}^{(2)} + \mathcal{C}_{\rm nfr}^{(0)}\hat{c}_{\rm nfr}^{(2)}}{\mathcal{F}^{(0)}}. \tag{B.2c}$$

Here we have singled out the fragmentation contributions in each SDC, which are encapsulated in the coefficients $\tilde{f}^{(1)}$ and $\tilde{f}^{(2)}$:

$$\tilde{f}^{(1)} = \frac{4\mathfrak{f}^{(1)}}{\mathcal{F}^{(0)}}\mathcal{C}_{\rm fr}, \qquad \tilde{f}^{(2)} = \frac{6\left(\mathfrak{f}^{(1)}\right)^2 + 4\mathfrak{f}^{(2)}}{\mathcal{F}^{(0)}}\mathcal{C}_{\rm fr}, \tag{B.3}$$

defined by the fragmentation contribution multiplied by the radiative corrections to the J/ψ decay constant.

$\cos\theta$	$\mathcal{F}^{(0)}$	$f^{(1)}$	$\tilde{f}^{(1)}$	$f^{(2)}$	$\tilde{f}^{(2)}$
0.999	4.76	-10.78	-11.40	-130.394-0.123=-130.52	-139.65
0.970	4.14	-10.89	-11.27	-129.370-0.172=-129.54	-138.08
0.872	1.60	-11.19	-11.90	-126.868-0.670=-127.54	-145.70
0.775	0.94	-11.37	-12.55	-124.802-1.429=-126.23	-153.77
0.677	0.65	-11.47	-13.20	-123.136-2.354=-125.49	-161.67
0.531	0.43	-11.51	-14.11	-121.319-3.853=-125.17	-172.76
0.384	0.33	-11.48	-14.88	-120.211-5.246=-125.46	-182.30
0.287	0.29	-11.45	-15.30	-119.781-6.006=-125.79	-187.39
0.140	0.26	-11.40	-15.72	-119.465-6.779=-126.24	-192.57
0	0.25	-11.38	-15.86	-119.364-7.032=-126.40	-194.27

TABLE B.1: Numerical values of various SDCs in (B.1) through $\mathcal{O}(\alpha_s^2)$ for ten different values of $\cos\theta$.

For reader's convenience, in Table B.1 we summarize various SDCs through $\mathcal{O}(\alpha_s^2)$ in the traditional NRQCD framework. In the second to last column in Table B.1, we split $f^{(2)}$ into two pieces which have different origin: the first piece includes the fragmentation and interference contributions, and the second term represents the non-fragmentation contribution $\mathcal{C}_{\rm nfr}^{(0)}\hat{c}_{\rm nfr}^{(2)}/\mathcal{F}^{(0)}$ in (B.2c). Note only the LO SDC $\mathcal{F}^{(0)}$ exhibits strong angular dependence, while the normalized higher-order SDCs $f^{(1,2)}$ have mild angular dependence.

The striking observation is that in a wide range of $\cos\theta$, the order-α_s SDC $f^{(1)}$ is well saturated by $\tilde{f}^{(1)}$, and $f^{(2)}$ is reasonably approximated by $\tilde{f}^{(2)}$. Since $\tilde{f}^{(i)}$ $(i = 1, 2)$ characterize the perturbative corrections to the J/ψ decay constant, the bulk contribution of the fixed-order perturbative corrections to the double-J/ψ cross section in standard NRQCD factorization actually arises from the perturbative corrections to the J/ψ decay constant. Because the perturbative corrections to $f_{J/\psi}$ in Eq. (8) become increasingly negative, it is not surprising to encounter the negative NLO and NNLO radiative corrections to $\sigma(e^+e^- \to J/\psi J/\psi)$ in the standard NRQCD factorization. In contrast, in our improved NRQCD approach, the predicted cross section at each perturbative order is always positive.

It worth noting that the higher-order contributions in the traditional NRQCD approach exhibit stronger μ_R dependence than that in the improved NRQCD approach. The key reason is that the perturbative convergence in the former is much worse than the latter.